

Supporting Information

Electrocatalytic CO₂ Reduction to Alcohols with High Selectivity over Two-Dimensional Fe₂P₂S₆ Nanosheet

Lei Ji,^{†,§,#} Le Chang,^{†,#} Ya Zhang,^{†,§} Shiyong Mou,[†] Ting Wang,^{⊥,†} Yonglan Luo,^{*,⊥} Zhiming Wang,[†] and Xuping Sun^{*,†}

[†]Institute of Fundamental and Frontier Sciences, University of Electronic Science and Technology of China, Chengdu 610054, Sichuan, China, [§]College of Chemistry, Sichuan University, Chengdu 610064, Sichuan, China, and [⊥]Chemical Synthesis and Pollution Control Key Laboratory of Sichuan Province, College of Chemistry and Chemical Engineering, China West Normal University, Nanchong 637002, Sichuan, China

[#]L.J. and L.C. contributed equally to this work

*E-mail: luoylcwnu@hotmail.com (Y.L.); xpsun@uestc.edu.cn (X.S.)

Experimental Section

Materials: Elemental iron (Fe, 99.99%, Sigma Aldrich, USA), red phosphorus powder (P, 100 mesh, 99%, Alfa Aesar, USA), potassium bicarbonate (KHCO_3), and sulfur (S, 99.98%, Aldrich, USA) were purchased. Analytical grade acetone was purchased from Fisher Scientific and it was distilled and used for the exfoliation of layered $\text{Fe}_2\text{P}_2\text{S}_6$. The sealing system (PPS-90, MRVS-1002) was purchased from Partulab Technology Co. Ltd. The water use throughout all experiments was purified through a Millipore system.

Preparation of bulk $\text{Fe}_2\text{P}_2\text{S}_6$ and $\text{Fe}_2\text{P}_2\text{S}_6$ nanosheet: Bulk $\text{Fe}_2\text{P}_2\text{S}_6$ was obtained by heating the mixture (about 0.5 g in total) of elements (Fe, P and S with 99.99% purity) in the required stoichiometric ratio in evacuated ($\sim 10^{-4}$ Pa) quartz tube at 700 °C at a ramping rate of 1 °C min^{-1} and held at this temperature for 6 days. $\text{Fe}_2\text{P}_2\text{S}_6$ nanosheets were prepared by exfoliation of bulk crystals. Briefly, 30 mg of the bulk crystals were dispersed in 10 mL of distilled acetone and sonicated for 4 h by ultrasonic cell disruptor. The moderately stable colloidal dispersions were centrifuged at 3000 rpm for 15 mins to remove bulky, unexfoliated material. Very stable, clear supernatant containing large quantities of $\text{Fe}_2\text{P}_2\text{S}_6$ nanosheets was obtained. Next, 500 μL of the obtained solution was added into 480 μL H_2O containing 20 μL of 5 wt% Nafion and sonicated for 1 h by normal ultrasonic instrument. Then 20 μL catalyst ink was loaded on a $1 \times 1 \text{ cm}^2$ carbon paper and dried under ambient condition, the catalyst loading mass is 0.1 mg.

Characterizations: XRD data were obtained from a LabX XRD-6100 X-ray diffractometer with Cu $\text{K}\alpha$ radiation (40 kV, 30 mA) of wavelength 0.154 nm (SHIMADZU, Japan). XPS measurements were performed on an ESCALABMK II X-ray photoelectron spectrometer using Mg as the exciting source. SEM images were collected from the tungsten lamp-equipped SU3500 scanning electron microscope at an accelerating voltage of 20 kV (HITACHI, Japan). TEM images were obtained from a Zeiss Libra 200FE transmission electron microscope operated at 200 kV. ^1H NMR spectra were collected on NMR spectrometer (Bruker AVANCEAV III HD 500) and

dimethyl sulphoxide was used as an internal to calibrate the chemical shifts in the spectra. Pre-saturation method was used to suppress water peak.

Electrochemical measurements: All electrochemical measurements were conducted using a CHI660E potentiostat (CH Instruments, China) in an H-type electrochemical cell separated by a Nafion 117 membrane, where graphite rod as the counter electrode and Ag/AgCl as the reference electrode. A mass flow controller was used to set the CO₂ flow rate at 30 sccm. All potentials measured were calibrated to RHE using the following equation: $E(\text{RHE}) = E(\text{Ag/AgCl}) + 0.61 \text{ V}$. All electrolytes were saturated by Ar or CO₂ bubbles before and during the experiments. Polarization curves were obtained using LSV with a scan rate of 2 mV s⁻¹. The long-term durability test was performed using chronopotentiometric measurements.

GC analysis: Detection and quantification of possible products was performed on an SHIMADZU GC-2014C gas chromatograph system equipped with two flame ionization detectors, one thermal conductivity detector and headspace auto-sampling sampler (COLINTech AutoHS). Separation was achieved using a DB-WAX column (100% polyethylene glycol, 30 m long with a 0.53 mm i.d. and 1.0 μm film thickness) and aluminium oxide column.

Ion chromatography: Detection and quantification of possible products (HCOO⁻) was performed on a Metrohm 940 professional ion chromatograph system.

Calculations of FE for H₂, methanol, and ethanol: FE was determined using the following equation:

$$\text{FE} = \frac{\text{Amount of electrons required to form the products}}{\text{Total amount of electrons supplied to system}} \times 100\%$$

Density functional theory calculations (DFT) calculation details: DFT calculations were performed with the spin-polarized planewave method implemented in the Quantum Espresso packag.¹ The Perdew–Burke–Ernzerhof (PBE) functional based on the generalized gradient approximation (GGA) were employed to evaluate the non-local exchange-correlation (xc) energy.² In a cubic supercell, the values of 40 and 400 Ry were used as the kinetic energy cutoff for wave functions and charge densities. The current work employs the Fe₂P₂S₆ surface. The possible positions of the atoms in

the complex were fully optimized until the forces were smaller than 0.01 eV Å⁻¹ per atom. The first Brillouin zone was sampled at the G point, and the electronic levels were broadened with a Gaussian smearing of about 0.002 Ry.³ The self-consistent field calculation has convergence criteria of 10⁻⁶ Hartree. The spin-polarization calculation was considered throughout the DFT calculation. A computational hydrogen electrode (CHE) was used to establish a free energy profile for electrochemical reduction reactions, as pioneered by Nørskov and co-workers.⁴ Briefly, to convert electronic energies to free energies, zero-point energy, enthalpy and entropy corrections of adsorbates were calculated using a harmonic oscillator approximation at 298.15 K. In details, Gibbs free energy is defined:

$$\Delta G = \Delta E + \Delta E_{\text{ZPE}} - T\Delta S$$

where ΔE represents the variation of the reaction energy obtained from DFT calculations as the expression: $\Delta E = E_{\text{AB}} - E_{\text{A}} - E_{\text{B}}$, where ΔE_{ZPE} is zero-point energy (ZPE) difference between the products and reactants in the reaction whose expression is similar to ΔE , where T represents the temperature ($T = 298.15$ K), and ΔS represents the change of entropy. For molecules, free energy corrections are taken from the reference.⁵

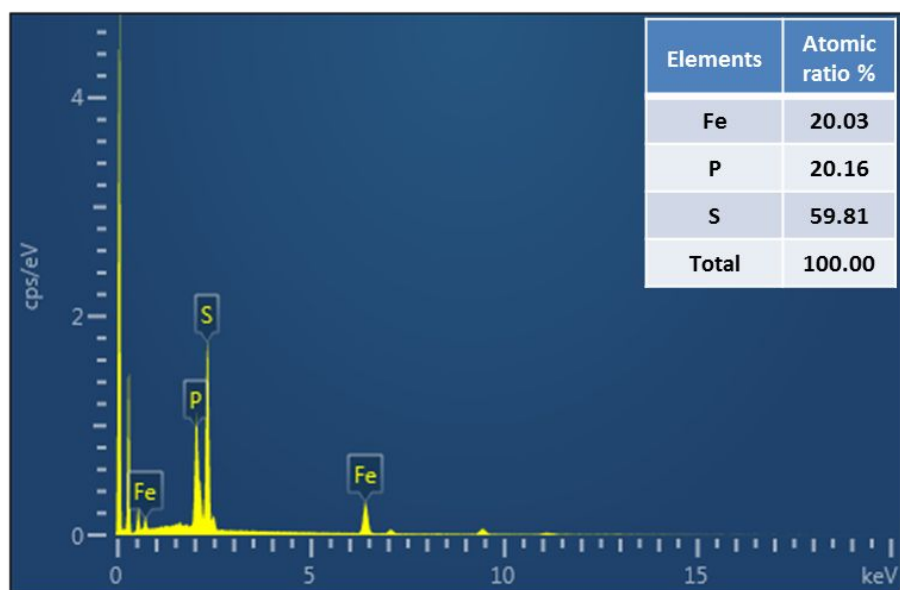


Figure S1. Energy dispersive X-ray spectrum of bulk $\text{Fe}_2\text{P}_2\text{S}_6$.

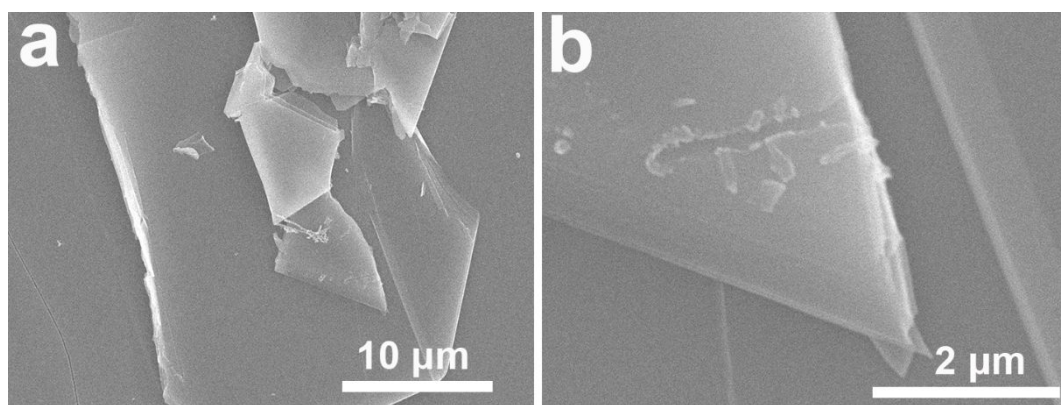


Figure S2. (a, b) SEM images of bulk Fe₂P₂S₆.

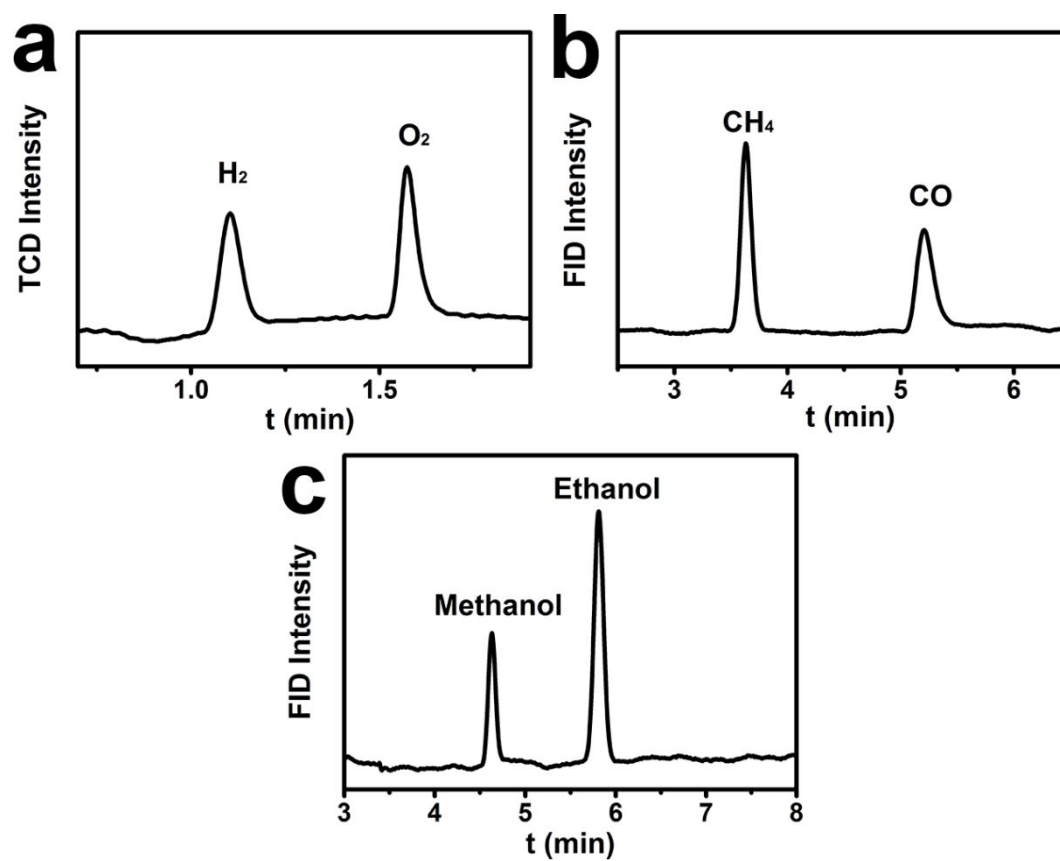


Figure S3. Typical chromatograms of H_2 , CH_4 , CO , methanol and ethanol measured by GC and HS-GC with FID.

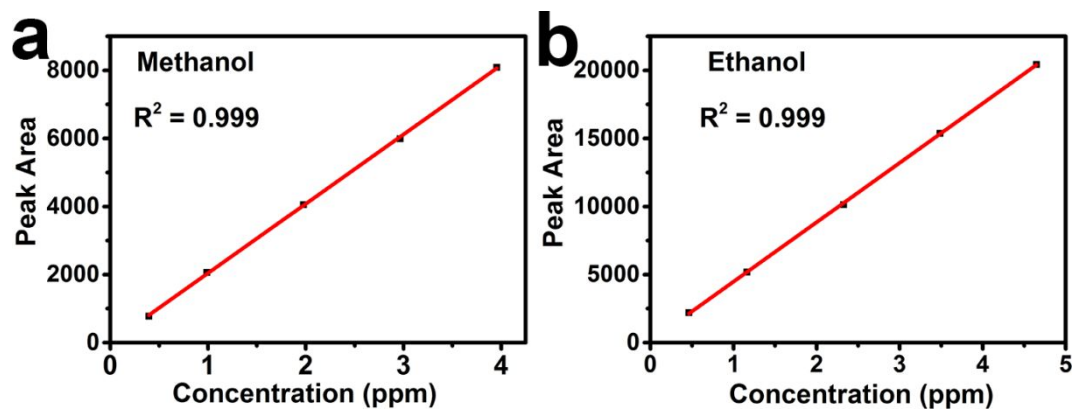


Figure S4. Standard calibration curves for (a) methanol and (b) ethanol.

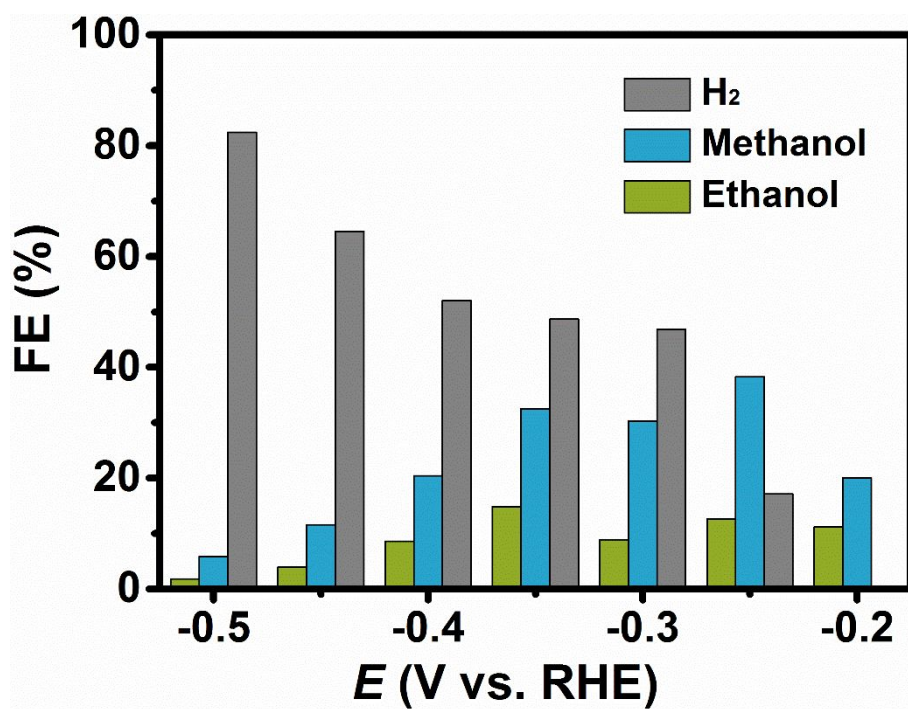


Figure S5. FEs of CO₂RR products on bulk Fe₂P₂S₆/CP at different potentials.

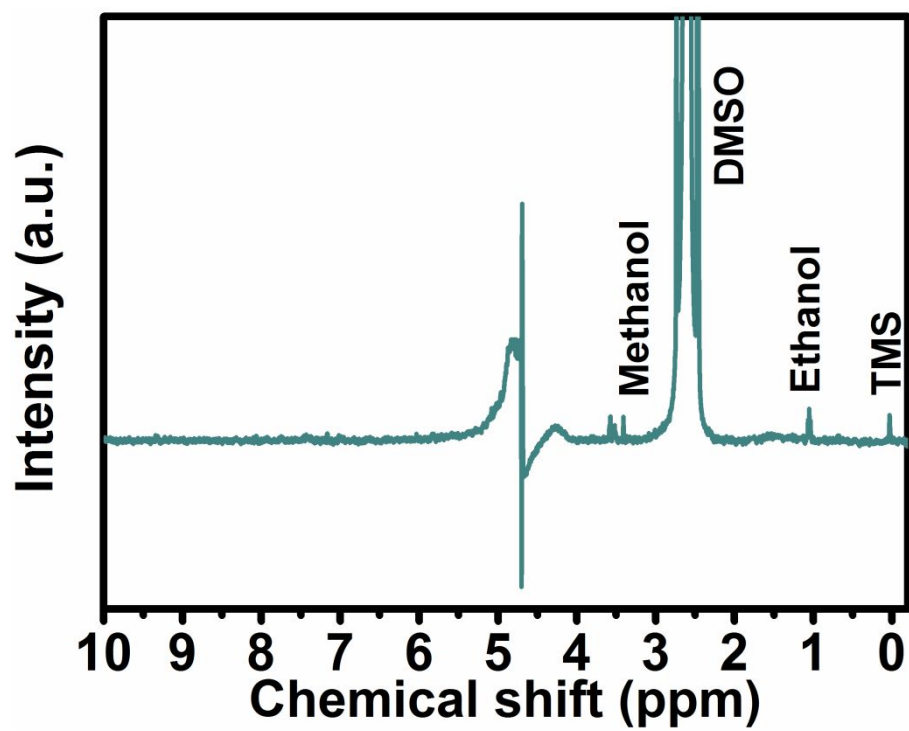


Figure S6. ^1H NMR spectrum of electrolyte after CO_2RR .

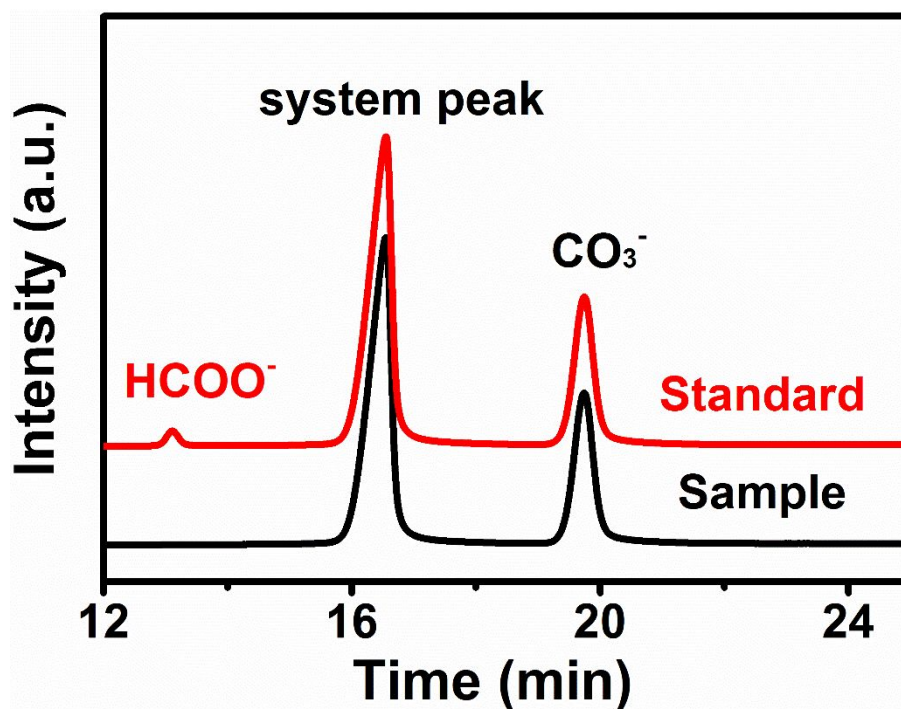


Figure S7. Ion chromatograms of standard sample (2.936 ppm HCOO⁻ in 0.5 M KHCO₃ solution) and the electrolyte after 2-h electrolysis.

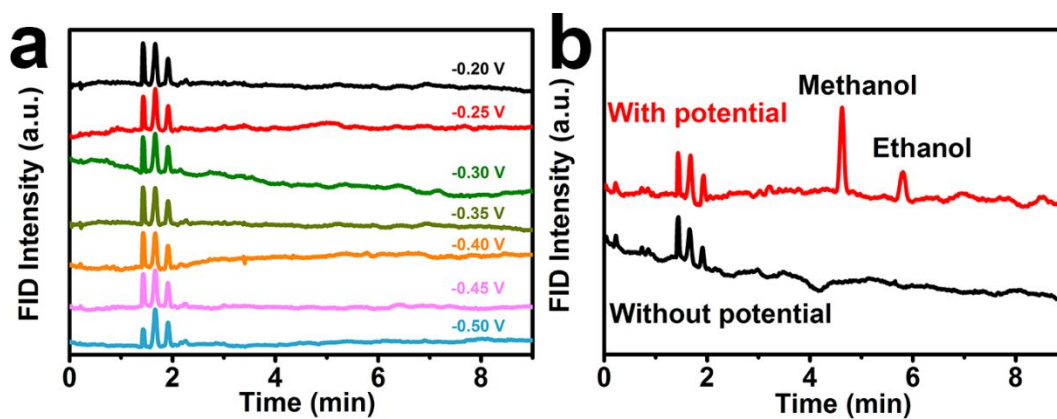


Figure S8. (a) Chromatograms for Ar-saturated 0.5 M KHCO_3 at different potentials using HS-GC. (b) Chromatograms for CO_2 -saturated 0.5 M KHCO_3 with and without potential applied to the electrochemical cell.

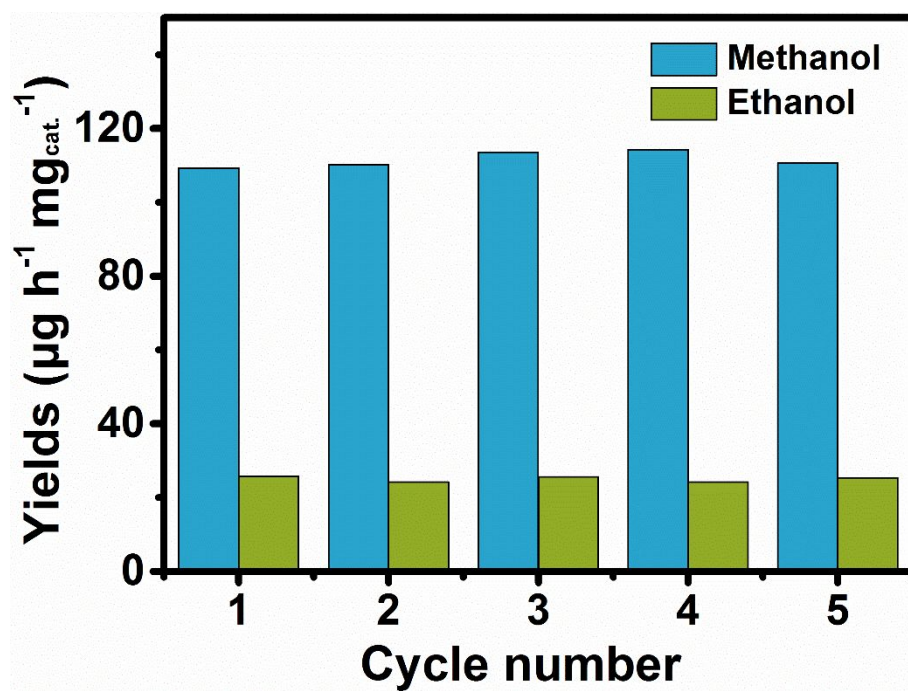


Figure S9. Alcohol yields on $\text{Fe}_2\text{P}_2\text{S}_6$ nanosheet/CP at applied potential -0.50 V for 5 times cycle measurements

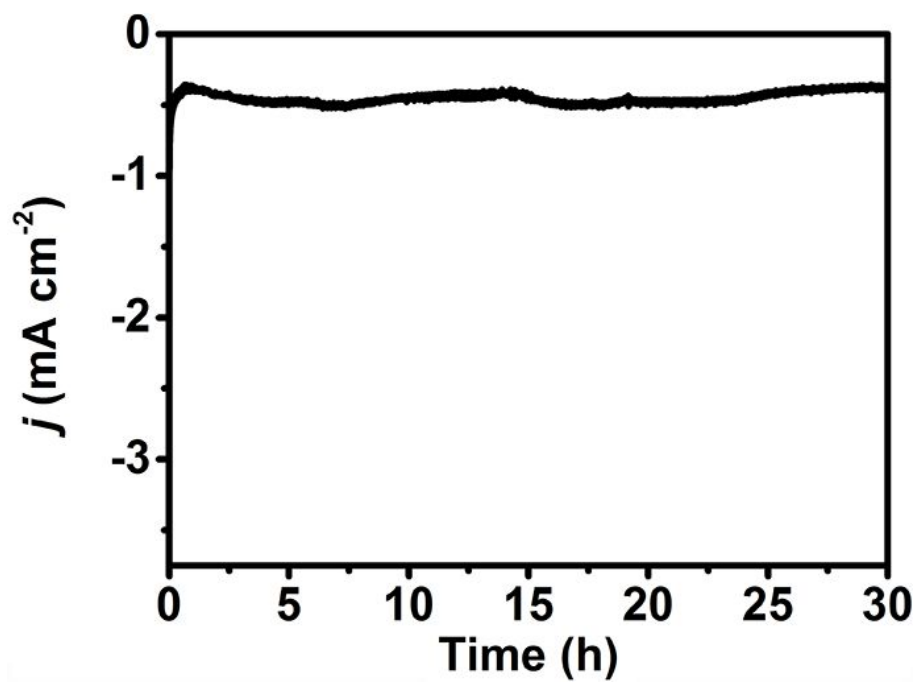


Figure S10. Chronopotentiometry curve under -0.50 V for 30 h in 0.5 M KHCO_3 .

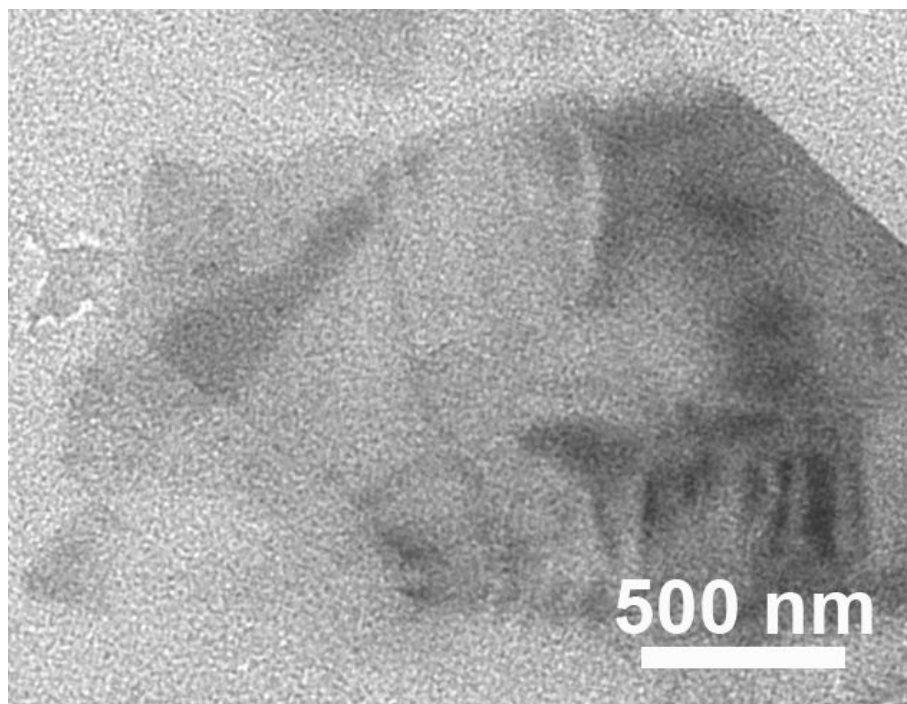


Figure S11. TEM image for Fe₂P₂S₆ nanosheet after long-term CO₂RR electrolysis.

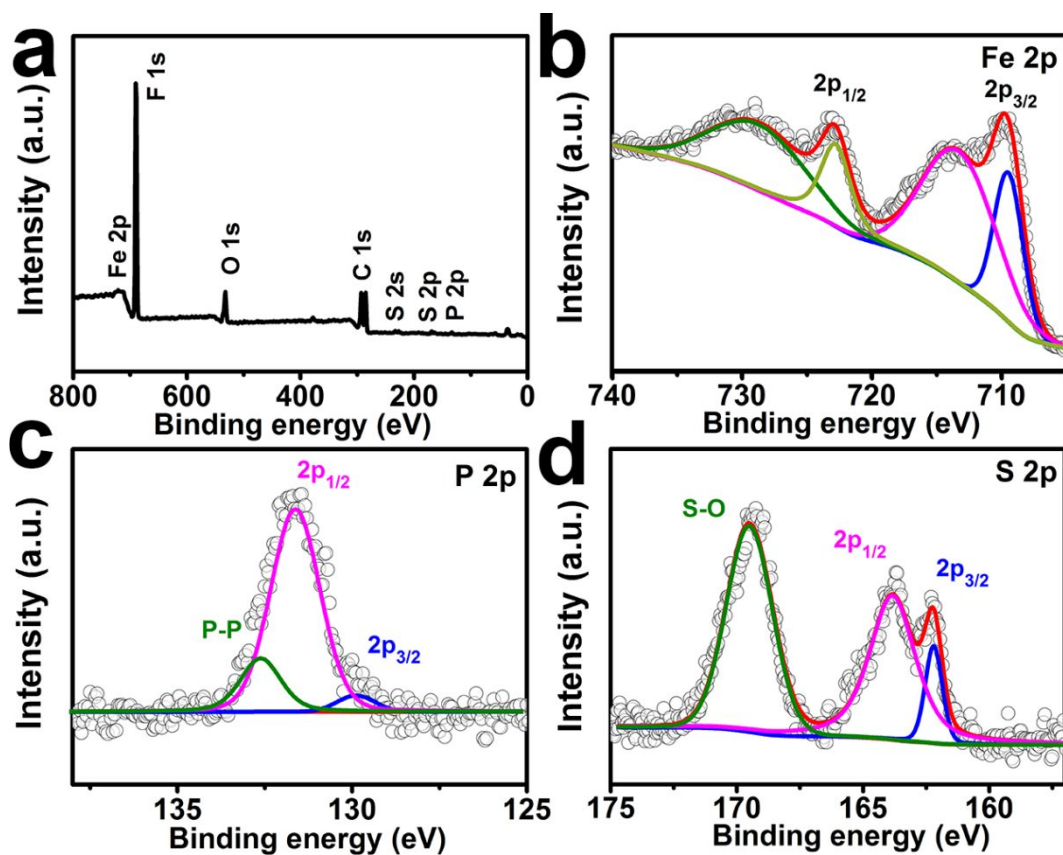


Figure S12. (a) XPS survey spectrum of Fe₂P₂S₆ nanosheet after long-term CO₂RR electrolysis. XPS spectra in (b) Fe 2p, (c) P 2p, and (d) S 2p regions for Fe₂P₂S₆ nanosheet. C 1s signals arise from carbon paper and Nafion. F element and S-O bond were attributed to Nafion.

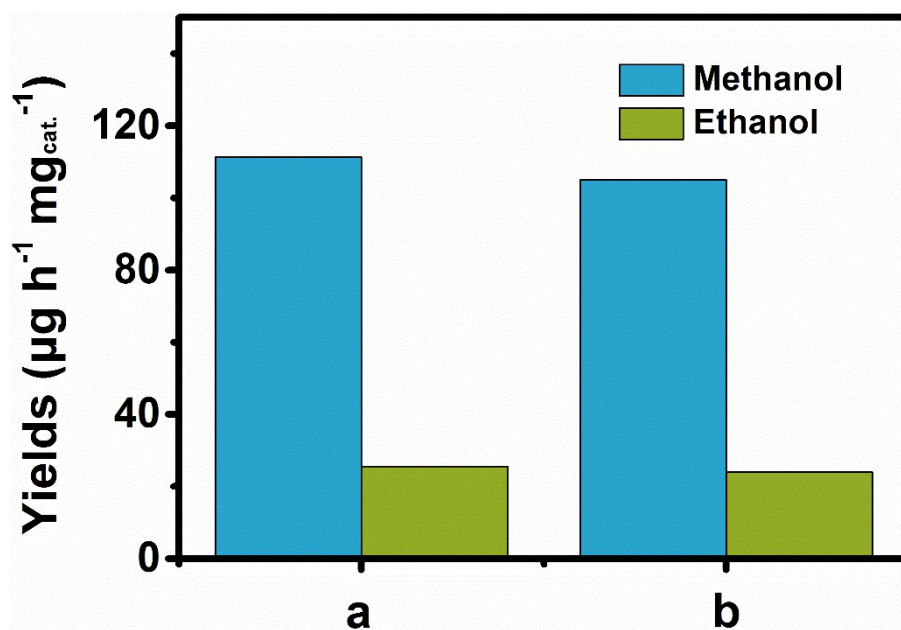


Figure S13. Yields of methanol and ethanol on Fe₂P₂S₆ nanosheet/CP before (a) and after (b) long-term electrolysis at -0.50 V for 2 h in 0.5 M KHCO₃.

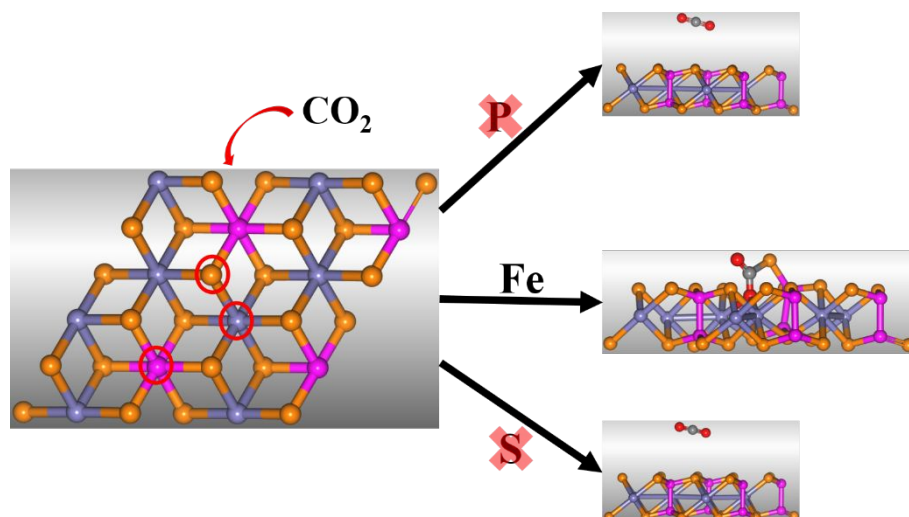


Figure S14. Tests on the active sites: P (pink), Fe (bluish violet), S (orange), O (red), and C (gray) atoms.

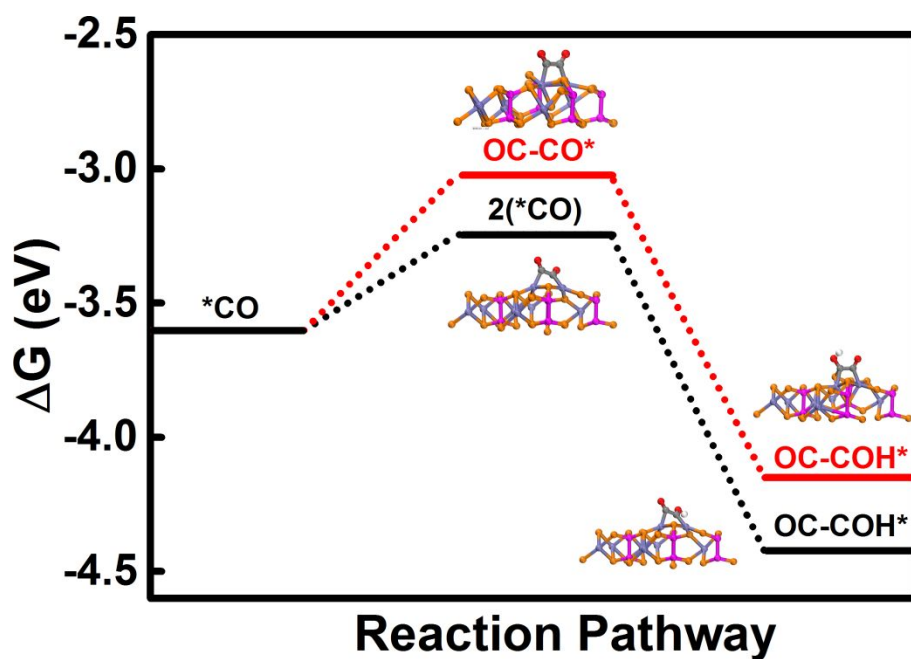


Figure S15. Reaction energy profile from DFT calculations for coupling path of CO + CO over $\text{Fe}_2\text{P}_2\text{S}_6$ surface. The nearby $\ast\text{CO}$ is coupled to form $2(\ast\text{CO})$ intermediate with ΔG of 0.35 eV. And the $\ast\text{CO}$ couples with the nearby $\text{CO}(\text{g})$ to form the intermediate OC-CO^\ast with ΔG of 0.57 eV. This implies that the intermediate $\ast\text{CO}$ is also available to combine another nearby $\text{CO}(\text{g})$ to produce the intermediate OC-CO^\ast and further hydrogenation into $\text{C}_2\text{H}_5\text{OH}$.

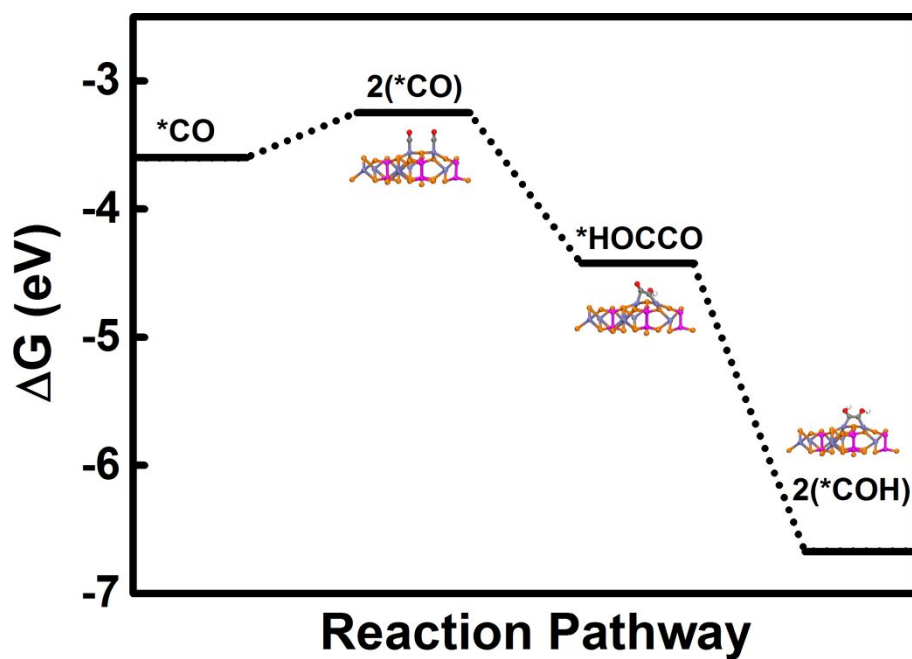


Figure S16. Reaction energy profile from DFT calculations for $2(*\text{CO}) \rightarrow 2(*\text{COH})$ stage over $\text{Fe}_2\text{P}_2\text{S}_6$ surface. The detailed $2(*\text{CO}) \rightarrow 2(*\text{COH})$ stage is considered in this work, where the H atom occurs to react subsequently.

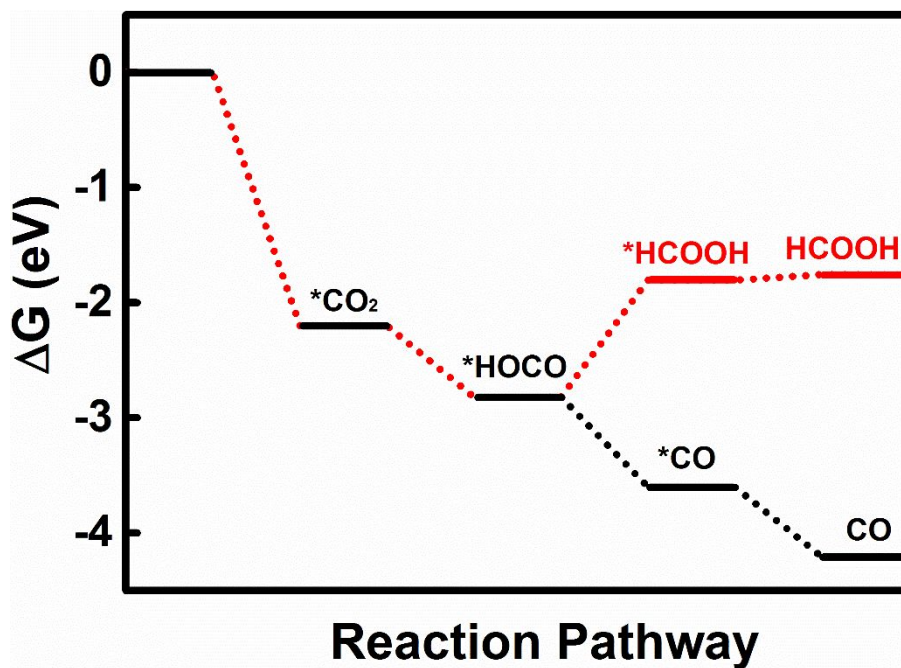


Figure S17. Reaction energy profile from DFT calculations for $*CO_2 \rightarrow *HCOO \rightarrow *HCOOH \rightarrow HCOOH$ stage over $Fe_2P_2S_6$ surface. The hydrogenation process of $*HOCO \rightarrow *HCOOH$ is an uphill pathway with $\Delta G = 0.97$ eV, implying that $*CO$ is preferentially generated in this reaction pathway rather than $*HCOOH$.

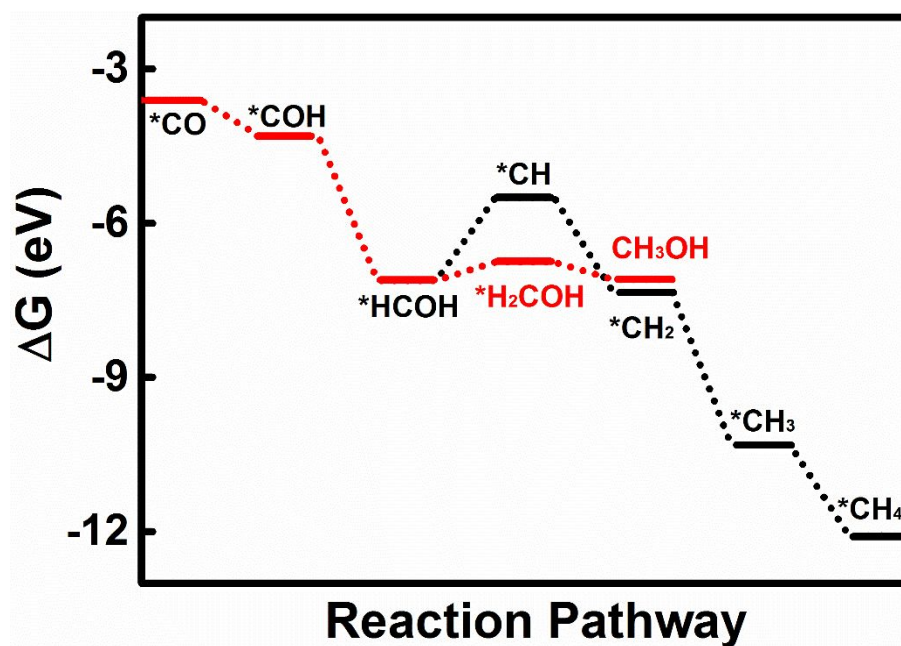
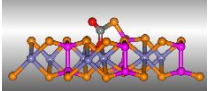
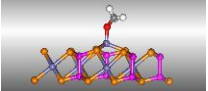
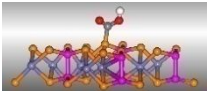
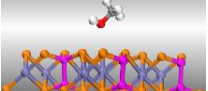
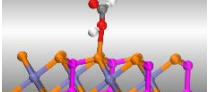
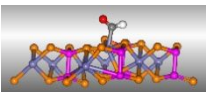
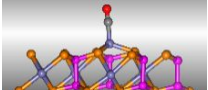
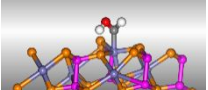
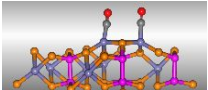
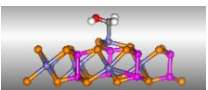
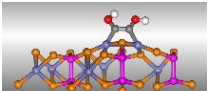
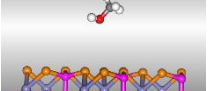
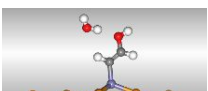
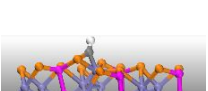
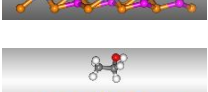

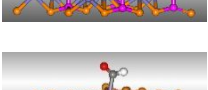
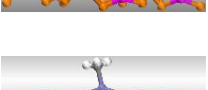
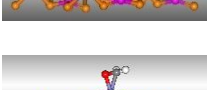
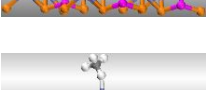


Figure S18. Reaction energy profile from DFT calculations for reaction pathway of CH₄ over Fe₂P₂S₆ surface. Processes of *HCOH → *CH and *HCOH → *H₂COH are uphill pathway with $\Delta G = 1.60$ eV and 0.36 eV, respectively. Thus, compared with *CH, the *HCOH preferentially converts to *H₂COH, which further hydrogenation into CH₃OH.

Table S1. Comparison of CO₂RR performance in aqueous media for Fe₂P₂S₆ nanosheet with other alcohol-producing electrocatalysts.

| Catalyst | Electrolyte | Potential (V) | FE (%) | | Ref. |
|---|------------------------------------|--------------------|----------|---------|-----------|
| | | | methanol | ethanol | |
| Fe ₂ P ₂ S ₆ nanosheet | 0.5 M KHCO ₃ | −0.20 vs. RHE | 65.2 | 23.1 | This work |
| Pd/SnO ₂ | 0.1 M NaHCO ₃ | −0.24 vs. RHE | 54.8±2 | - | (6) |
| Cu ₂ O/ZnO-based electrodes | 0.5 M KHCO ₃ | −1.3 V vs. Ag/AgCl | 17.7 | - | (7) |
| RuO ₂ -TiO ₂ nanoparticle | 0.5 M NaHCO ₃ | −0.8 V vs. SCE | 60.5 | - | (8) |
| Cu ₂ O-MWCNTs | 0.5 M NaHCO ₃ | −0.8 V vs. Ag/AgCl | 38 | - | (9) |
| Ru/Cu | 0.5 M NaHCO ₃ | −0.8 V vs. SCE | 41.3 | - | (10) |
| Cu(I) oxide | 0.5 M NaHCO ₃ | −1.1 V vs. SCE | 38 | - | (11) |
| Cu-Au alloy | 0.5 M NaHCO ₃ | −1.1 V vs. SCE | 15.9 | 12.0 | (12) |
| Cu Nanowire Arrays | 0.1 M KHCO ₃ | −1.1 V vs. SCE | - | 5.0 | (13) |
| Cu ₂ O films | 0.1 M KHCO ₃ | −0.99 V vs. RHE | - | 17.22 | (14) |
| Cu ₄ Zn | 0.1 M NaHCO ₃ | −1.05 V vs. RHE | - | 29.1 | (15) |
| Co/SL-NG | 0.1 M NaHCO ₃ | −0.90 V vs. SCE | 71.4 | - | (16) |
| Co(CO ₃) _{0.5} OH·0.11H ₂ O | 0.1 M NaHCO ₃ | −0.98 V vs. SCE | 97.0 | - | (17) |
| Cu ₈₈ Sn ₆ Pb ₆ alloy | 1.5 M HCl-0.17 M BaCl ₂ | −0.6 V vs. Ag/AgCl | 36.3 | - | (18) |
| [PYD]@Pd | 0.5 M KCl | −0.6 V vs. SCE | 35 | - | (19) |
| [PYD]@Cu-Pt | 0.5 M KCl | −0.6 V vs. SCE | 37 | - | (20) |
| [PYD]@Cu-Pd | 0.5 M KCl | −0.6 V vs. RHE | - | 12±1 | (21) |

Table S2. All of the species during the reaction pathways. Fe, bluish violet; P, pink; S, orange; O, red; C, gray; H, white.

| Species | Geometry | Species | Geometry |
|-----------------------------------|---|---------------------------------|--|
| *CO ₂ |  | *OCH ₃ |  |
| *HOCO |  | CH ₃ OH ¹ |  |
| *HCOOH |  | *COH |  |
| *CO |  | *HCOH |  |
| *2(CO) |  | *H ₂ COH |  |
| *2(COH) |  | CH ₃ OH ² |  |
| *C ₂ H ₂ OH |  | *CH |  |
| C ₂ H ₅ OH |  | *CH ₂ |  |
| *HCO |  | *CH ₃ |  |
| *OCH ₂ |  | *CH ₄ |  |

Reference

- (1) Giannozzi, P.; Baroni, S.; Bonini, N.; Calandra, M.; Car, R.; Cavazzoni, C.; Ceresoli, D.; Chiarotti, G. L.; Cococcioni, M.; Dabo, I.; Corso, A. D.; de Gironcoli, S.; Fabris, S.; Fratesi, G.; Gebauer, R.; Gerstmann, U.; Gougoussis, C.; Kokalj, A.; Lazzeri, M.; Martin-Samos, L.; Marzari, N.; Mauri, F.; Mazzarello, R.; Paolini, S.; Pasquarello, A.; Paulatto, L.; Sbraccia, C.; Scandolo, S.; Sclauzero, G.; Seitsonen, A. P.; Smogunov, A.; Umari, P.; Wentzcovitch, R. M. QUANTUM ESPRESSO: A Modular and Open-Source Software Project for Quantum Simulations of Materials. *J. Phys. Condens. Matter* **2009**, *21*, 395502.
- (2) Perdew, J. P.; Burke, K.; Ernzerhof, M. Generalized Gradient Approximation Made Simple. *Phys. Rev. Lett.* **1996**, *77*, 3865–3868.
- (3) Methfessel, M.; Paxton, A. T. High-Precision Sampling for Brillouin-Zone Integration in Metals. *Phys. Rev. B* **1989**, *40*, 3616–3621.
- (4) Nørskov, J. K.; Rossmeisl, J.; Logadottir, A.; Lindqvist, L. Origin of the Overpotential for Oxygen Reduction at a Fuel-Cell Cathode. *J. Phys. Chem. B* **2004**, *108*, 17886–17992.
- (5) Peterson, A. A.; Abild-Pedersen, F.; Studt, F.; Rossmeisl, J.; Nørskov, J. K. How Copper Catalyzes the Electroreduction of Carbon Dioxide into Hydrocarbon Fuels. *Energy Environ. Sci.* **2010**, *3*, 1311–1315.
- (6) Zhang, W.; Qin, Q.; Dai, L.; Qin, R.; Zhao, X.; Chen, X.; Ou, D.; Chen, J.; Chuong, T.; Wu, B.; Zheng, N. Electrochemical Reduction of Carbon Dioxide to Methanol on Hierarchical Pd/SnO₂ Nanosheets with Abundant Pd–O–Sn Interfaces. *Angew. Chem. Int. Ed.* **2018**, *57*, 9475–9479.
- (7) Albo, J.; Sáez, A.; Solla-Gullón, J.; Montie, V.; Irabien, A. Production of Methanol from CO₂ Electroreduction at Cu₂O and Cu₂O/ZnO-Based Electrodes in Aqueous Solution. *Appl. Catal. B: Environ.* **2015**, *176–177*, 709–717.
- (8) Qu, J.; Zhang, X.; Wang, Y.; Xie, C. Electrochemical Reduction of CO₂ on RuO₂/TiO₂ Nanotubes Composite Modified Pt Electrode. *Electrochim. Acta* **2005**, *50*, 3576–3580.

- (9) Malik, M. I.; Malaibari, Z. O.; Atieh, M.; Abussaud, B. Electrochemical Reduction of CO₂ to Methanol over MWCNTs Impregnated with Cu₂O. *Chem. Eng. Sci.* **2016**, *152*, 468–477.
- (10) Popić, J. P.; Avramov-Ivić, M. L.; Vuković, N. B. Reduction of Carbon Dioxide on Ruthenium Oxide and Modified Ruthenium Oxide Electrodes in 0.5 M NaHCO₃. *J. Electrochem. Soc.* **1997**, *421*, 105–110.
- (11) Le, M.; Ren, M.; Zhang, Z.; Sprunger, P. T.; Kurtz, R. L.; Flake, J. C. Electrochemical Reduction of CO₂ to CH₃OH at Copper Oxide Surfaces. *J. Electrochem. Soc.* **2011**, *158*, E45–E49.
- (12) Jia, F.; Yu, X.; Zhang, L. Enhanced Selectivity for the Electrochemical Reduction of CO₂ to Alcohols in Aqueous Solution with Nanostructured Cu-Au Alloy as Catalyst. *J. Power Sources* **2014**, *252*, 85–89.
- (13) Ma, M.; Djanashvili, K.; Smith, W. A. Controllable Hydrocarbon Formation from the Electrochemical Reduction of CO₂ over Cu Nanowire Arrays. *Angew. Chem. Int. Ed.* **2016**, *55*, 6680–6684.
- (14) Ren, D.; Deng, Y.; Handoko, A. D.; Chen, C. S.; Malkhandi, S.; Yeo, B. S. Selective Electrochemical Reduction of Carbon Dioxide to Ethylene and Ethanol on Copper(I) Oxide Catalysts. *ACS Catal.* **2015**, *5*, 2814–2821.
- (15) Ren, D.; Ang, B. S.-H.; Yeo, B. S. Tuning the Selectivity of Carbon Dioxide Electroreduction toward Ethanol on Oxide-Derived Cu_xZn Catalysts. *ACS Catal.* **2016**, *6*, 8239–8247.
- (16) Huang, J.; Guo, X.; Yue, G.; Hu, Q.; Wang, L. Boosting CH₃OH Production in Electrocatalytic CO₂ Reduction over Partially Oxidized 5 nm Cobalt Nanoparticles Dispersed on Single-Layer Nitrogen-Doped Graphene. *ACS Appl. Mater. Interfaces* **2018**, *10*, 44403–44414.
- (17) Huang, J.; Hu, Q.; Guo, X.; Zeng, Q.; Wang, L. Rethinking Co(CO₃)_{0.5}(OH)·0.11H₂O: A New Property for Highly Selective Electrochemical Reduction of Carbon Dioxide to Methanol in Aqueous Solution. *Green Chem.* **2018**, *20*, 2967–2972.

- (18) Schizodimou, A.; Kyriacou, G. Acceleration of the Reduction of Carbon Dioxide in the Presence of Multivalent Cations. *Electrochim. Acta* **2012**, *78*, 171–176.
- (19) Yang, H.; Qin, S.; Wang, H.; Lu, J. Organically Doped Palladium: A Highly Efficient Catalyst for Electroreduction of CO₂ to Methanol. *Green Chem.* **2015**, *17*, 5144–5148.
- (20) Yang, H.; Yue, Y.; Qin, S.; Wang, H.; Lu, J. Selective Electrochemical Reduction of CO₂ to Different Alcohol Products by an Organically Doped Alloy Catalyst. *Green Chem.* **2016**, *18*, 3216–3220.
- (21) Yang, H.; Qin, S.; Yue, Y.; Liu, L.; Wang, H.; Lu, J. Entrapment of a Pyridine Derivative within a Copper–Palladium Alloy: A Bifunctional Catalyst for Electrochemical Reduction of CO₂ to Alcohols with Excellent Selectivity and Reusability. *Catal. Sci. Technol.* **2016**, *6*, 6490–6494.